ELSEVIER

Earth and Planetary Science Letters 128 (1994) 113–121

EPSL

Anelastic tomography: a new perspective on upper mantle thermal structure

Barbara Romanowicz

Seismographic Station and Department of Geology and Geophysics, University of California at Berkeley, Berkeley, CA 94720, USA

Received 2 June 1994; accepted 30 August 1994

Abstract

Anelastic tomography provides new insights into the thermal structure of the earth's upper mantle. Lateral variations in Q are largest in the upper 300 km, but remain significant down to at least 500–600 km. They correlate with the distribution of plates in the upper 300 km, in agreement with cooling plate models and with the distribution of hotspots at greater depths. Two major upwellings are revealed under Hawaii and northeastern Africa, which may originate at the bottom of the transition zone or deeper. Low Q structure beneath the main ridge systems, on the other hand, does not appear to extend vertically below about 300 km.

1. Introduction

It has often been emphasized that global velocity tomography is a powerful tool for mapping temperature fluctuations associated with mantle convection [1,2]. In particular, the distribution of velocities in the lowermost 1000 km of the mantle appear to be reasonably well explained by invoking hot rising currents correlated with the surface distribution of hotspots and cold sinking currents representing the remnants of subducted slabs. However, tomographic models of the upper mantle transition zone do not show such clear correlations, particularly not with hotspots. In consequence, the depth of origin of hot rising plumes underlying hotspots is still a matter of debate [3].

There is now, however, general agreement that the physical mechanism most likely to be responsible for intrinsic attenuation in the earth's mantle consists of a distribution of thermally activated relaxation mechanisms [4] and, therefore, the temperature dependence of the quality factor, Q, in the mantle is exponential, of the form $\exp(H^*/RT)$, where T is temperature, R is the gas constant and H^* is activation enthalpy [5]. This is borne out by experimental data, at least in the temperature ranges currently accessible [5,6]. We therefore expect that lateral variations in temperature in the mantle should be strongly expressed in Q, especially emphasizing hotter than average regions. Thus, in the upper mantle, hot rising plumes could be more easily detectable in Q models.

Lateral variations in upper mantle Q attain on the order of 50–100% [7–10], in contrast to only a few percent in velocity fluctuations [11,12]. Yet attenuation tomography is lagging behind that of elastic velocities because of serious difficulties encountered in measuring anelastic attenuation accurately. Indeed, elastic velocity information is extracted from the phase of seismic waves, which behaves linearly along the propagation path, to a

SSDI 0012-821X(94)00191-X

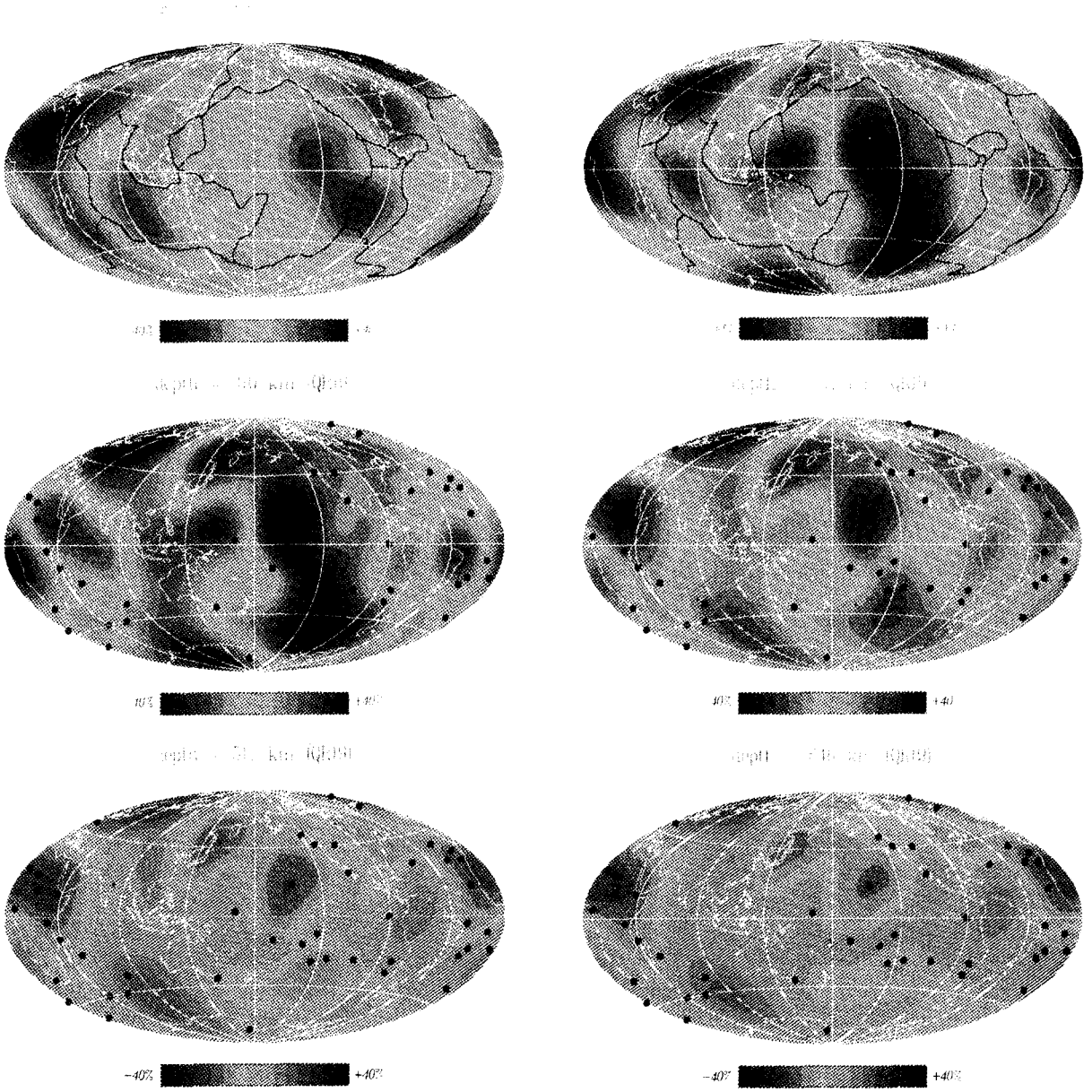

Fig. 1. Lateral variations in shear attenuation at representative depths in the upper mantle. The maps represent relative deviations (in %) from the mean at each depth in terms of Q, with red standing for low Q (hot) regions and blue for high Q (cold) ones. The distribution of hotspots according to a standard selection [24] has been superimposed on the maps at and below 310 km. The measurement method is described in detail elsewhere [18]. The inversion proceeds in two steps: (1) measurements of $\eta(\omega)$ on individual source station paths are inverted to obtain 2D maps of lateral variations in Q^{-1} at a set of discrete frequencies and associated error maps. The continuous inversion method of Tarantola and Valette [19] is used, with a correlation length of 3000 km, corresponding roughly to the resolution of a degree 6 spherical harmonics expansion. This optimal correlation length is determined empirically from the data coverage (similar to that shown in [10]); (2) the set of 2D maps, in the period range 120–300 sec, is inverted with depth, also using the continuous inversion method, with correlation lengths varying from 50 km, at the top of the model, to 100 km in the transition zone. The resulting errors are uniformly distributed at each depth and average $\sim \pm 15\%$ at 100 km, $\pm 10\%$ at 200 km, $\pm 13\%$ at 310 km, $\pm 14\%$ at 444 km, $\pm 15\%$ at 555 km and $\sim \pm 23\%$ at 670 km. The map at 670 km is given for reference, although fundamental mode Rayleigh waves have limited power to determine whether the similarities in the features observed at 444 km and 670 km are real or a result of smearing over this depth range. The model has been tested for stability by performing inversions using different subsets of the entire data set.

very good approximation. On the other hand, amplitude, from which Q information is derived, is strongly and non-linearly affected by focusing and other 'off-path' effects due to propagation in complex structures. Separation of elastic and anelastic effects in the amplitude involves, in principle, accurate knowledge of the 3D elastic structure and sophisticated non-linear forward modelling techniques [13]. Because of these fundamental problems, global 3D models of lateral variations in Q have so far been limited to tectonic regionalizations [8,9], or low degree, incomplete models, derived from free oscillation [14–16] or great circle average measurements [10,17] which resolve only components symmetric with respect to the center of the earth.

I have recently developed a new technique to measure Q for mantle Rayleigh waves travelling on individual minor and major arcs [18] and have applied it to data from GEOSCOPE and IRIS networks from the periods 1987–1993 and 1989–1993, respectively. The period range for measurements is 80–320 sec. The philosophy underlying this technique recognizes that current elastic models are not accurate enough in their description of transverse gradients of structure to allow accurate forward modelling of focusing effects. These effects also become stronger with the orbit number of the wavetrain. The technique therefore relies on the use of first arriving trains and a severe data selection to eliminate those paths which appear to be severely affected by focusing. The size of the resulting data set is relatively small ($\sim$ 500–900 paths, depending on the period) and spatial resolution is inferior to that of current elastic models. Nevertheless, both odd and even order lateral heterogeneity is resolved and instabilities, as well as spurious symmetries, are avoided by the use of an inversion method [19,20] which does not rely on a specific set of basis functions (such as spherical harmonics) but only on the specification of an optimal spatial correlation length.

Here, I discuss the prominent features of the resulting three-dimensional model of upper mantle Q. This is the first model of resolution comparable to a complete degree 6 spherical harmonics expansion. A detailed discussion of technical aspects involved in the construction of this model is presented elsewhere [Romanowicz, in prep.].

2. The upper mantle Q model

Samples of the 3D model at representative depths are given in Fig. 1. The 3D variations in Q have several striking features. The upper mantle can be divided into two distinct domains, with a transition at depths of 250–350 km. Above 300 km, the pattern follows the distribution of continents and oceans, with minima centered near ridges: East Pacific Rise, mid-Atlantic Ridge, Indian Ocean and maxima associated with stable continental regions and the Pacific rim. Other prominent low Q regions comprise back arcs in the western Pacific and a broad region around Hawaii. Within the spatial resolution of this model (equal or larger than $\sim$ 3000 km), this is well correlated with tectonic features, heat flow distribution [21] and elastic wave velocities [11,12]. However, the 'hotter than average' region around Hawaii is not apparent in tomographic velocity models.

While lateral variations are largest around 200–300 km and decrease at greater depth, in agreement with what was found by Durek et al. [17], I find that significant heterogeneity in Q persists into the transition zone. The variance reduction in the second part of the inversion (inversion with depth) increases from 31.5% if the model is restricted to a maximum depth of 250 km, to 39.2%, 46.4%, 48.1% and 48.9% if the depth range is extended to 350, 450, 550 and 650 km, respectively. The marginal increase in variance reduction beyond 550 km reflects the loss of sensitivity with depth of the fundamental mode in the period range considered. It is, therefore, not possible to determine whether significant lateral variations in Q actually exist beyond 500–600 km.

The deep pattern, which prevails below a depth of about 300 km, is notably different from the shallower pattern, in agreement with what is found on a more regional scale [22]. There are two strong minima in Q, centered on Hawaii and the northern part of the African continent. Overall, low Q regions correspond well with the

hotspot distribution on the surface of the earth [23,24] (Fig. 1). This correlation is comparable to that found between hotspots and the low velocity regions in tomographic maps of the lower mantle [1]. Such a correlation is not obvious in transition zone velocity models, which correlate better with the slab geoid model [1,24].

The similarities and differences with velocity tomographic results in the transition zone are instructive. In Fig. 2, I have plotted the variation with depth of various correlation coefficients for models of velocity and Q. Both are correlated with heat flow in the first 300 km. Below 300 km, the correlation of Q with heat flow is replaced by one with hotspots, and that of velocity by one with the slab model. The correlation of velocity with hotspots is marginal throughout the mantle. Fig. 3 shows the strong correlation with age of the seafloor in the southern Pacific and southern Atlantic Ocean in the depth range 100–250 km. Notably, this correlation vanishes below a depth of 300 km, reflecting the change in global spatial pattern below that depth.

The 3D picture of the upper mantle thermal structure that emerges from the Q and velocity tomography is in agreement with a model of mantle dynamics in which the cooling of lithospheric plates dominates the temperature field in the shallow parts [25]. The deeper patterns are, on the other hand, related to the deep mantle circulation and reflect both downwelling associated with sinking slabs and upwelling originating from a deep, hot boundary layer whose most direct expression at the surface is through hotspots. Because of the exponential dependence of Q on temperature, the Q tomography emphasizes hot rising currents, while velocity tomography emphasizes cold — slab related — downwellings, since the negative temperature contrast associated with sinking slabs is expected to be larger than the positive one associated with upwellings at transition zone depths, at least if the hot bottom boundary layer is located deeper than 500–600 km.

Another difference between the distribution of velocity and Q in the upper mantle is that lateral

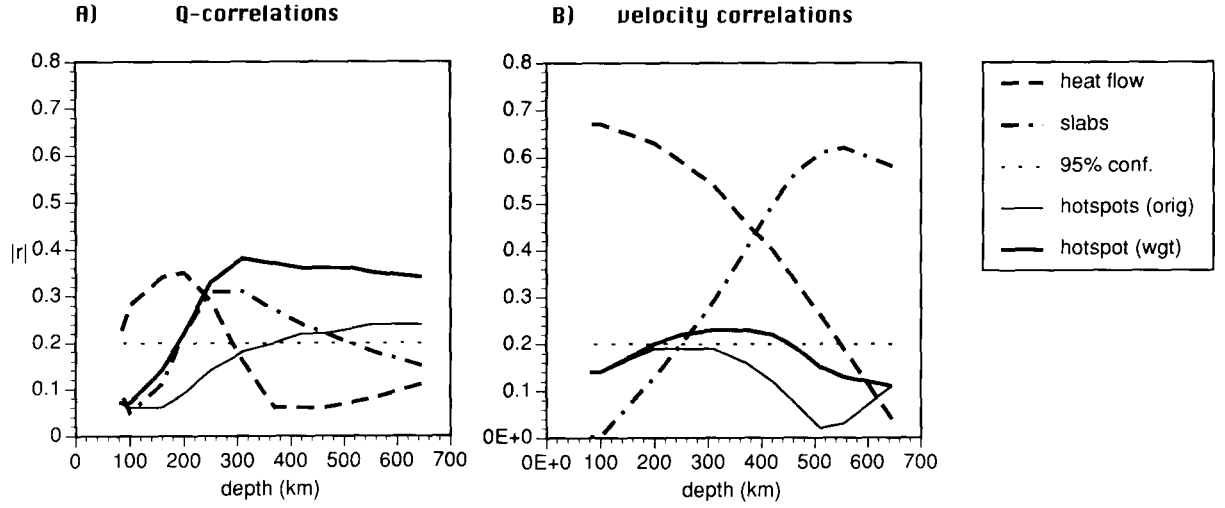

Fig. 2. Correlations with heat flow, slabs and hotspot distribution of (a) the Q model of Fig. 1 and (b) the velocity model of Woodward et al. [12]. The correlation coefficient (given here in absolute value) is calculated according to:

$$r = \Sigma_l \Sigma_m (C_{lm} a_{lm} + S_{lm} b_{lm}) / \sqrt{\left[\left(\Sigma C_{lm}^2 + S_{lm}^2 \right) \left(\Sigma a_{lm}^2 + b_{lm}^2 \right) \right]}$$

where (C_{lm}, S_{lm}) and (a_{lm}, b_{lm}) are the spherical harmonics expansion coefficients of each of the models being compared, with the summation being for $l = 1$–6. Correlations with hotspot distribution [24] are shown for 2 cases: (1) hotspots equally weighted (orig.); (2) hotspots weighted according to buoyancy strength [29] (wgt) as described in Fig. 4. Dashed lines indicate 95% confidence limits on the significance of the correlations for degree 6 expansions.

variations in velocity are largest in the lithosphere, decrease with depth and sharply drop in amplitude beneath depths of 200–300 km [11,12], while those in Q appear to peak around 300 km. If the lateral variations in Q do, indeed, represent lateral variations in temperature, the relatively increased level of fluctuations in elastic velocity in the first 200 km is likely to be due to the combined effect of temperature and chemical composition, the latter potentially contributing up to 50% of the lateral velocity variations [26,27].

3. The Hawaiian and African plumes

Below 300 km, the 3D distribution of attenuation presents two absolute maxima: over Hawaii and northeastern Africa. The importance of the Hawaian hotspot is not totally unexpected. In calculations of buoyancy fluxes underneath hotspot swells [28,29], Hawaii stands out stronger by at least a factor of two with respect to any other single hotspot. It is also known for the distinctive, more 'primitive' isotopic signature of

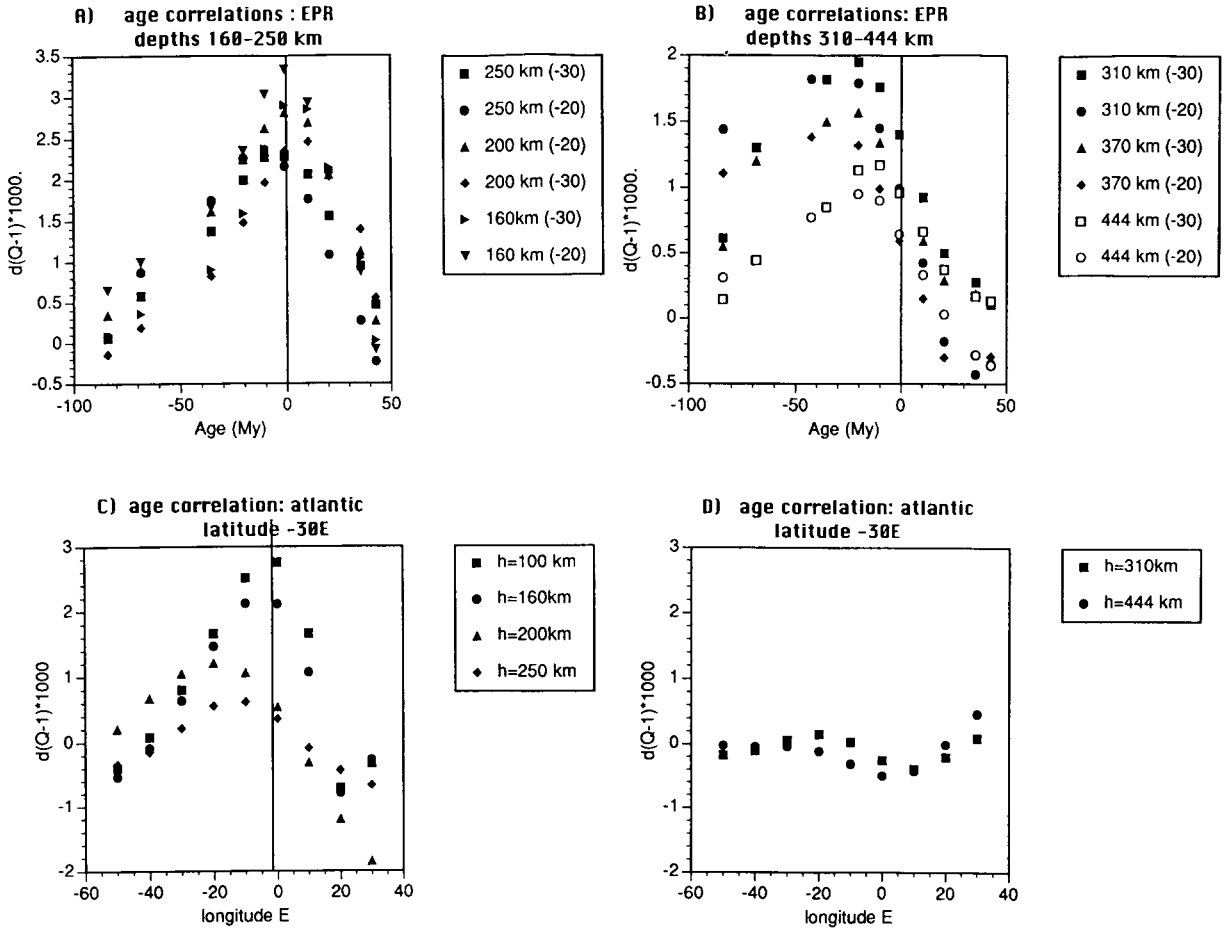

Fig. 3. (a) Correlation of Q^{-1} anomaly with age of the sea floor on both sides of the East Pacific Rise, at latitudes of 20°S to 30°S, in the depth range 100–250 km. Circles are for the west side and squares for the east side of the ridge, revealing an asymmetry associated with the low Q region in the central Pacific (Fig. 1). (b) same as (a) for the depth range 300–500 km. Note that in (b) the maximum anomaly is displaced to the west with respect to the ridge axis by about 25°. (c) and (d) same as (a) and (b) for the southern Atlantic Ocean, at a latitude of −30°S. Note that in (c) and (d) the axis is actually longitude, not age. The correlation decreases with depth and is not seen below 250 km.

its ocean ridge basalts (OIB) [30]. On the other hand, although extended rifting, volcanism and high heat flow is a distinctive feature of north-eastern Africa, a direct correspondence with upwelling currents at transition zone depths has, until now, not been possible because it is not apparent in velocity tomography. While limited in resolution, the 3D Q model presented here indicates a possible link between the strength of individual or groups of hotspots and the location of the main upwellings in the global convective circulation. In Fig. 4, I compare spherical harmonics expansions, up to degree 6, of the hotspot distribution weighted according to different schemes. The standard approach is to give equal weights to all hotspots, which is mathematically convenient, but not necessarily justified from a geodynamics point of view. In fact, the correlation with the Q^{-1} maps at transition zone depths, shown in Fig. 2, improves when replacing the distribution of hotspots with equal weights (Fig. 4, upper) by one in which each hotspot is weighted according to buoyancy strength, as estimated by Sleep et al. [29] (Fig. 4, middle). The latter weighting scheme has a more solid physical basis because it recognizes the large variability in hotspot tectonic setting and activity. Assuming laboratory inferred values for the activation energy, the temperature contrasts between the center of the upwelling and the background mantle in the transition zone are of the order of 200–300 K, in good agreement with estimates based on calculations of thermal fluxes of plumes [29]. The resolution in the Q model is insufficient to allow a more quantitative assessment of the individual hot spot strengths but this comparison indicates that African hotspots may be the surface expression of at least one major upwelling current in the mantle. To improve the correlation further, it is necessary to decrease the strength of individual south Pacific hotspots (Tahiti, Marquesas, Pitcairn and MacDonald) and increase (Fig. 4 bottom) the strength of the African hotspots (Afar, Lake Victoria, Mt Cameroon, Tibesti and Hoggar). This exercise is, at the present stage, somewhat arbitrary but the point here is that 3D Q models have potential to constrain the dynamic characteristics of different hotspots around the world. For example, only the Hawaian hotspot has so far been singled out for its buoyancy and geochemical characteristics, while extended rift-

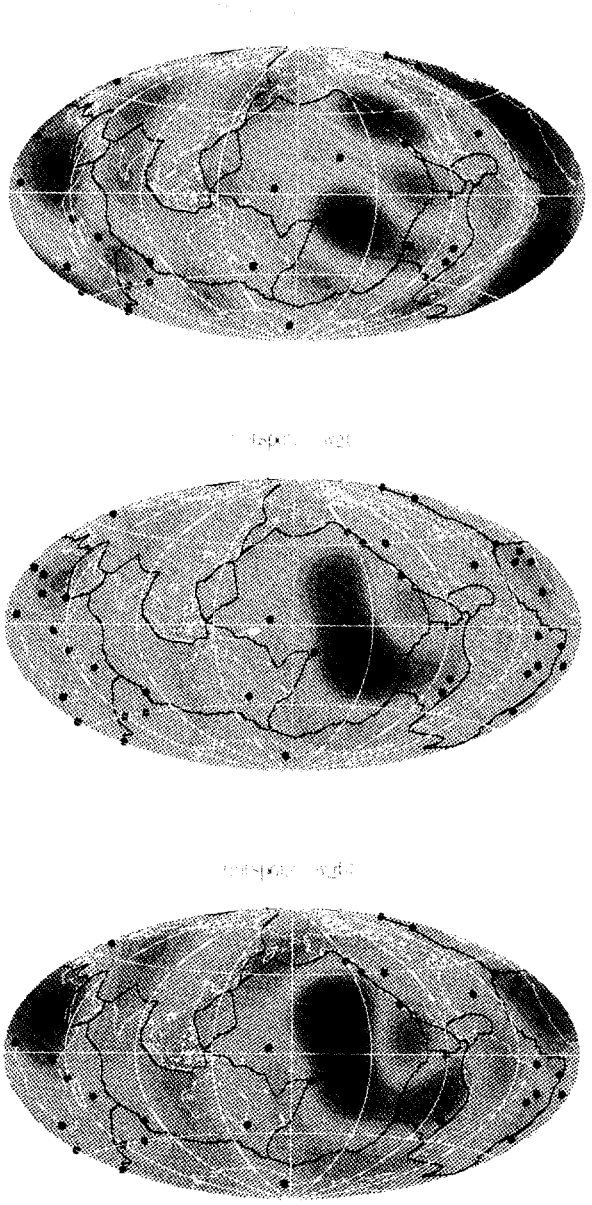

Fig. 4. Spherical harmonics expansion, up to degree and order 6 (term $l = 0$ excluded), of the hotspot distribution [24], weighted according to different schemes. Upper: equal weights for all hotspots. Middle: weights according to buoyancy strength [29]. Lower: modified from the former to match the locations of the maxima in the attenuation maps in Fig. 1.

ing, volcanism and heat flow anomalies are well known on the African continent. If the inference made from the present Q model is borne out by future independent studies, this may indicate that plate velocity is not the only factor that needs to be taken into account in the estimation of hot spot plume strength and, in this particular instance, the interaction between the hot plume, or system of plumes with the cold and thick African lithosphere, needs to be reconsidered.

Having established a relation between the observed hotspots and upwellings in the transition zone, I now discuss how the latter may relate to current models of hotspot plumes and recent numerical models of global mantle circulation. Even though the very low Q regions beneath the central Pacific and northern Africa may represent a smeared version of much narrower currents, they must be wide enough to be detected by surface waves whose wavelength is of the order of 1000 km. It is therefore not strictly appropriate to call them 'plumes', since the classical geophysical meaning of this term implies narrow conduits of diameter not exceeding 200–400 km [31]. In this context, the category of plume 'heads' may be more appropriate, implying a widening of the hot plume conduit in the upper mantle, as a consequence of plume dynamics [31] and through their interaction with lithospheric plates [32]. On the other hand, numerical convection calculations indicate that plumes play a minor role in the heat budget of the earth and recent models tend to emphasize the importance of cold downwellings and the inhibiting role of the 670 km discontinuity for currents of either direction to penetrate across the upper mantle/lower mantle boundary [33–35]. In this context, the two largest Q minima may represent two exceptional hot upwellings that are strong enough to penetrate into the upper mantle. Upon encountering lithospheric plates, these upwellings break up into narrower conduits leading up to individual hotspots, while the bulk of the heat is deflected towards ridges. This may explain, in particular, why no Q minima are present under North Africa down to 250 km: the narrow hot conduits are imbedded in the bulk of cold continental lithosphere and are beyond the resolution of the present Q model. This is in qualitative agreement with the argumentation of Zhang and Tanimoto [36], who appear to have detected such conduits beneath a number of hotspots in the first 100 km of depth in a high resolution velocity tomographic study. However, the depth range in which the deflection towards ridges occurs is much deeper than proposed by these authors, of the order of 200–350 km, as seen in Fig. 3 and in agreement with other elastic tomographic results [11,12]. This depth range is marked by a maximum in the amplitude of the degree 2 pattern in Q, as well as in velocity [10], which can be explained by a shift to low harmonics in the power spectrum of the temperature field occurring as a consequence of interaction of mantle flow with lithospheric plates [32].

4. Discussion

The model presented here is a crude first attempt at mapping 3D Q structure and the details will likely change as more accurate measurements of anelastic attenuation become possible in the future, contingent on the availability of more accurate elastic models. Nevertheless, the change in pattern between shallow and deep parts of the upper mantle is well within the resolution of the current model. Also, the general distribution of the deeper anomalies, with peaks in attenuation in the central Pacific and in North Africa is stable and to some extent corroborated, at least in its longest wavelength features, by independent normal mode studies [14–16].

The tomographic Q model presented here gives the first evidence for hot upwellings at transition zone depths associated with surface hotspots. These upwellings must originate in a hot boundary layer located deeper than the asthenosphere, possibly around or even beneath the 670 km discontinuity. It is not possible at this time, to constrain the depth of this boundary layer further. It is worth noting also that there is a correspondence between the geographical location of the two strongest attenuation maxima and that of the two strongest minima in velocity models, below depths of 1600–2000 km [12,37]. The correlation of the lowermost mantle velocity lows with

hotspots has been frequently pointed out [1]. It is tempting to relate the transition zone upwellings to these velocity lows but there remains a missing piece of the puzzle; namely, that there is no clear indication of strong upwellings in current velocity models in the depth range 700–1600 km. If they do exist, the corresponding hot zones cannot be detected in velocity models, either because they are reduced to narrow plumes in this depth range or because slab signature is still dominant. By the time they reach the lower third of the mantle, slabs will have equilibrated their temperature with the surrounding mantle. The positive temperature contrast due to hot upwellings from the bottom boundary layer will then have larger amplitude, allowing velocity tomography to detect them.

Further constraints on the depth of the boundary layer at which hotspot plumes originate and on plume geometry must await more accurate 3D models of Q, including lower mantle ones: a challenge for the future.

Acknowledgements

This paper has benefitted from discussions with L. Kellogg and S. Karato, as well as helpful reviews by D. Yuen and M. Ritzwoller. The study was supported under NSF grant EAR-9204631. It is U.C. Berkeley Seismographic Station contribution #200. [RV]

References

[1] B.H. Hager, R.W. Clayton, M.A. Richards, R.P. Comer and A.M. Dziewonski, Lower mantle heterogeneity, dynamic topography and the geoid, Nature 313, 541–545, 1985.

[2] P. Olson, P.G. Silver and R.W. Carlson, The large-scale structure of convection in the Earth's mantle, Nature 344, 209–215, 1990.

[3] J. Morgan, Convection plumes in the lower mantle, Nature 230, 42–43, 1971.

[4] D.L. Anderson and J.B. Minster, The physics of creep and attenuation in the mantle, in: Anelasticity in the Mantle, AGU Geodyn. Ser. 4, 5–11, 1981.

[5] W. Kampfmann and H. Berkhemer, High temperature experiments on the elastic and anelastic behaviour of magmatic rocks, Phys. Earth. Planet. Inter. 40, 223–247, 1985.

[6] I. Jackson, M.S. Paterson and J.D. FitzGerald, Seismic wave dispersion and attenuation in Aheim dunite: an experimental study, Geophys. J. Int. 108, 517–534, 1992.

[7] N. Jobert and G. Roult, Periods and damping of free oscillations observed in France after sixteen earthquakes, Geophys. J. R. Astron. Soc. 45, 155–176, 1978.

[8] I. Nakanishi, Regional differences in the phase velocity and the quality factor Q of mantle Rayleigh waves, Science 200, 1379–1381, 1978.

[9] A.M. Dziewonski and J. Steim, Dispersion and attenuation of mantle waves through waveform inversion, Geophys. J. R. Astron. Soc. 70, 503–527, 1983.

[10] B. Romanowicz, The Upper Mantle Degree 2: constraints and inferences from global mantle wave attenuation measurements, J. Geophys. Res. 95, 11,051–11,071, 1990.

[11] J.P. Montagner and T. Tanimoto, Global upper mantle tomography of seismic velocities and anisotropies, J. Geophys. Res. 96, 20,337–20,351, 1991.

[12] R.L. Woodward, A.M. Forte, W.J. Su and A.M. Dziewonski, in: Chemical Evolution of the Earth and Planets, AGU Geophys. Monogr. 74, 89–109, 1993.

[13] Ph. Lognonne, Normal modes and seismograms in an anelastic rotating Earth, J. Geophys. Res. 96, 20,309–20,319, 1991.

[14] N. Suda, N. Shibata and Y. Fukao, Degree-2 pattern of attenuation structure in the upper mantle from apparent complex frequency measurements of fundamental spheroidal modes, Geophys. Res. Lett. 18, 1119–1122, 1991.

[15] M.F. Smith and G. Masters, Aspherical structure constraints from free oscillation frequency and attenuation measurements, J. Geophys. Res. 94, 1953–1976, 1989.

[16] G. Roult, B. Romanowicz and J.P. Montagner, 3D upper mantle shear velocity and attenuation from fundamental mode free oscillation data, Geophys. J. Int. 110, 61–80, 1990.

[17] J. Durek, M. Ritzwoller and J.H. Woodhouse, Constraining upper mantle anelasticity using surface wave amplitude anomalies, Geophys. J. Int. 114, 249–272, 1993.

[18] B. Romanowicz, On the measurement of anelastic attenuation using amplitudes of low frequency surface waves, Phys. Earth Planet. Inter. 84, 179–192, 1994.

[19] A. Tarantola and B. Valette, Generalized non-linear inverse problems solved using the least squares criterion, Rev. Geophys. 20, 219–232, 1982.

[20] J.P. Montagner, Regional three-dimensional structures using long-period surface waves, Ann. Geophys. 4B3, 283–294, 1986.

[21] D.S. Chapman, Continental heat flow, in: Landolt–Bornstein Numerical Data and Functional Relationships in Science and Technology, New Series Vol. 2, K. Fuchs and H. Soffel, eds., pp. 1–19, Springer, Berlin, 1985.

[22] M. Bussy, J.P. Montagner and B. Romanowicz, Tomo-

graphic study of upper mantle attenuation in the Pacific Ocean, Geophys. Res. Lett. 20, 663–666, 1993.
[23] Crough T., Hotspot swells, Ann. Rev. Earth Planet. Sci. 11, 165–193, 1983.
[24] M.A. Richards, B.H. Hager and N.H. Sleep, Dynamically supported geoid highs over hotspots: observation and theory, J. Geophys. Res. 93, 7690–7708, 1988.
[25] G.F. Davies, Mantle plumes, mantle stirring and hotspot geochemistry, Earth Planet. Sci. Lett. 99, 94–109, 1990.
[26] B. Yan, E.K. Graham and K.P. Furlong, Lateral variations in upper mantle thermal structure inferred from three-dimensional seismic inversion models, Geophys. Res. Lett. 16, 449–452, 1989.
[27] S.-I. Karato, Importance of anelasticity in the interpretation of seismic tomography, Geophys. Res. Lett. 20, 1623–1626, 1993.
[28] G.F. Davies, Ocan bathymetry and mantle convection 1. Large scale flow and hotspots, J. Geophys. Res. 93, 10,467–10,480, 1988.
[29] N. Sleep, Hotspots and mantle plumes: some phenomenology, J. Geophys. Res. 95, 6715–6736, 1990.
[30] W.M. White, Sources of oceanic basalts: radiogenic isotope evidence, Geology 13, 115–118, 1985.
[31] P. Olson, G. Schubert and Ch. Anderson, Structure of axisymmetric mantle plumes, J. Geophys. Res. 98, 6829–6844, 1993.
[32] M. Gurnis and S. Zhong, Generation of long wavelength heterogeneity in the mantle by the dynamic interaction between plates and convection, Geophys. Res. Lett. 18, 581–584, 1991.
[33] P. Tackley, D.J. Stevenson, G.A. Glazmaier and G. Schubert, Effects of an endothermic phase transition at 670 km depth in a spherical model of convection in th Earth's mantle, Nature 361, 699–704, 1993.
[34] W.R. Peltier and L.P. Solheim, Mantle phase transitions and layered chaotic convection, Geophys. Res. Lett. 19, 321–324, 1992.
[35] S. Honda, S. Balachandar, D.A. Yuen and D. Reuteler, Science 259, 1308–1311, 1993.
[36] Y.-S. Zhang and T. Tanimoto, Ridges, hotspots, and their interpretation as observed in seismic velocity maps, Nature 355, 45–49, 1992.
[37] X-D. Li and B. Romanowicz, Non-linear waveform inversion for global structure considering cross-branch coupling, EOS Trans Am. Geophys. Union 74, 557, 1993.